Received: 29 July 2024 | Revised: 13 September 2024 | Accepted: 13 December 2024 | Published online: 20 December 2024

RESEARCH ARTICLE

Journal of Optics and Photonics Research
2025, Vol. 2(2) 86–92
DOI: 10.47852/bonviewJOPR42023979

BON VIEW PUBLISHING

Differential Cross-Sections and Energy Shifts in Electron-Atom Scattering Under Linearly Polarized Laser Fields

Raju Bohora[1], Kishori Yadav[1] and Saddam Husain Dhobi[2,*]

[1]*Department of Physics, Tribhuvan University (Patan Multiple Campus), Nepal*

[2]*Central Department of Physics, Tribhuvan University, Nepal*

Abstract: This study investigates electron-atom scattering within linearly polarized laser field, employing the first-order Born approximation and perturbation theory for target dressing. The Hamiltonian integrates both unbound electron and atomic target in the laser field, with the electron's wave functions described by Gordon-Volkov waves. Elastic scattering for hydrogen atoms in various states (1s, 2s, 3s) is examined to determine differential cross-sections (DCS) and energy shifts. To study the nature of DCS and energy shifting, electric field strengths (1 to 4 a.u.), Bessel function orders (1 to 4), scattering angles (0 to 30 degrees), and laser energy (1.17 eV) are used in this research. Results indicate higher laser field strengths correlate with lower energy shifts, significantly impacting scattering dynamics, while DCS values decrease with increased scattering angles and higher Bessel function orders. The transitions involving higher orbital states show broader momentum ranges and smoother DCS decay. These findings elucidate the interplay between atomic structure, incident energy, and scattering characteristics, offering valuable insights for applications in plasma physics and materials science by aiding precise modeling of atomic interactions under varying conditions.

Keywords: electron-atom scattering, linearly polarized laser field, differential cross-sections, energy shifts, Gordon-Volkov waves, hydrogen atom states, Bessel function orders

1. Introduction

The Gravitational Behavior of Antihydrogen at Rest experiment, which examines the influence of gravity on antimatter, relies heavily on three-body collisions. A crucial difficulty is increasing the manufacturing rate, which is normally relatively low [1]. A laser field is employed to influence the collision process by applying a perturbative technique that combines the Coulomb-Born approximation with first-order perturbation theory [2]. Further research in the field involves the development of a distorted wave approach for atom structure calculations as well as collision dynamics in plasma environments [3] and advances in femtosecond laser-assisted electron scattering equipment [4], along with theoretical investigations through electron-light interactions in ultrafast electron microscopy, which might further enhance space-time-energy resolution [5].

When particles or waves encounter an obstruction or interact with other particles or fields, they are physically misdirected or deflected from their initial course, a phenomenon known as scattering. Considerable work has been devoted to investigating electron-atom scattering in the presence of a powerful laser field, including the experiment and the work [6, 7]. Mason [8] summarized the experimental situation of electron-atom scattering. Prior to Gersten's [9] work, the atomic target was described by a static potential. However, subsequent studies considered the laser dressing of the target, handling the radiation-atom interaction perturbatively. This approach was also adopted in the works [10, 11], and notably [12]. In all these investigations, a linearly polarized laser field was considered. The phenomenon of energy shift was first observed by Johannes Stark in 1913 when he discovered that the spectral lines of hydrogen atoms were split by an electric field, known as the Stark effect. Later, in 1933, Alfred Kastler and Jean Brossel observed that the energy levels of atoms were also shifted by a magnetic field [13].

Series of studies investigating the cross-sectional interactions between electrons and protons, as well as electrons and hydrogen atoms, under both laser and non-laser conditions [1–12]. Their research focuses on understanding the thermodynamics of thermal electrons, the impact of electron-ion interactions on output current in proton exchange membrane fuel cell (PEMFC), differential cross-sections (DCS) in inelastic scattering scenarios with weak laser fields, and the scattering dynamics of free electrons with hydrogen atoms within PEMFC systems. Their recent work has also explored DCS utilizing Volkov-Thermal wave functions in Coulomb potentials, contributing to a comprehensive understanding of these interactions around PEMFC electrodes [14, 15].

Scattering phenomena occur when particles or waves encounter obstructions or interact with other particles or fields, resulting in deflection from their initial course. Previous research has extensively investigated electron-atom scattering in the presence of powerful laser fields, providing both theoretical and experimental insights [6–8, 13, 16]. While these studies have predominantly focused on transitions between lower orbits

*Corresponding author: Saddam Husain Dhobi, Central Department of Physics, Tribhuvan University, Nepal. Email: saddam@ran.edu.np

(e.g., orbit 1 to 2), there is a gap in understanding transitions involving higher-order orbits, particularly in the context of a linearly polarized laser field. Additionally, the effects of laser field strength on energy shifts, initially observed by Johannes Stark in 1913 and further explored by Alfred Kastler and Jean Brossel in 1933, remain under-explored for higher-order transitions. The objective of this work is to study the DCS for electron transitions between higher-order orbits in a linearly polarized laser field and to analyze the corresponding energy shifts due to varying laser field strengths. This study attempts to close the current gap by extending transition investigations to higher-order orbits, providing new insights into scattering processes under the impact of powerful laser beams. This discovery is significant because it has the potential to improve understanding of electron-ion interactions along with energy shifts, contributing to developments in domains like PEMFCs as well as applications involving laser-atom interactions.

2. Methods and Materials

In the event of the existence of a laser field, the perturbed system can be represented as:

$$H = H_f + H_t + V_d \tag{1}$$

where V_d is the electrons-atom interaction under the direct channel, and H_f as well as H_t represent the Hamiltonians that represent the unbound electron along with the atomic target, respectively, in the presence of an intense laser field. The wave function generated by an unbound electron within the laser field is described by the Schrödinger equation [17]:

$$i\hbar\frac{\partial}{\partial \mathfrak{t}}\chi(r_o,t) = H_f\chi(r_o,t) = \frac{1}{2m}\left(p+\frac{e}{c}A\right)^2\chi(r_o,t) \tag{2}$$

where $\chi(r_0,t)$ is wavefunction of the electron, which is a function of position r_0 and time t, p is momentum, e is charge of electron, c is velocity of light, and A is vector potential. In the present work, we treat only single-mode laser field in the framework of the dipole approximation, considering the linearly polarized situation. The classical oscillations vector a(t) can be expressed as a(t) = $a_0\epsilon\sin(\omega t)$, whereas a($t$) reflects the electron's oscillations in the electric field $\epsilon(t)$. Functioning in the case of the Coulomb gauge, the vector of electromagnetic potential A(t) is given as A(t) = $A_0\cos(\omega t)$. Gordon-Volkov waves to describe both the beginning and the end states of the dispersed electron. The equivalent solution is given for an electron possessing kinetic energy (E_k), the electron wave vector k, as well as frequency ω [18, 19].

$$\chi_{\vec{k}}(\vec{r},t) = \frac{1}{(2\pi)^{\frac{3}{2}}}\exp\left\{i\left(k\cdot r_0 - k\cdot a_0\sin(\omega t) - \frac{E_k t}{\hbar}\right)\right\} \tag{3}$$

Here, $a_0 = \frac{\varepsilon_0}{\omega^2} = \frac{A_0}{c\omega}$, k is momentum, r_0 is position, E_k is kinetic energy of electron, and $\hbar$ bar is planks constant. We focus our analysis on high scattering energies where the first-order Born approximation provides highly accurate results. The electron-atom interaction, described by a static potential, is detailed in Cionga et al. [20] and Dhankhar et al. [21].

$$V(r,R) = -\frac{1}{r} + \frac{1}{|\vec{r}-\vec{R}|} \tag{4}$$

Here, $\vec{r}$ and $\vec{R}$ represent the position vectors of the electron and bound electron, respectively. We employ a semi-perturbative approach [22] for scattering. Our analysis commences with the scattering matrix, as discussed in the context of high-energy scattering [23].

$$S_{if}^{B1} = -i\int_{-\infty}^{+\infty} dt < \chi_{\vec{k}_f}(t)\psi_{nlm}(t)|V(r,R)|\chi_{\vec{k}_f}(t)\psi_{nlm}(t) > \tag{5}$$

where ψ_{nlm} is unperturbed excited state of hydrogen of energy E_n and $\chi_{\vec{k}_{i(f)}}$ is the Gordon-Volkov wave equation for initial and final states of scattering electron which are identical due to free-free transition. For high-energy projectile electrons $(E_{k_i} > 150\ eV)$, exchange effects can be safely omitted, and they are excluded from our scattering matrix calculations. We utilize a first-order time-dependent perturbation theory to examine the interaction of hydrogen atoms in these circumstances, assuming that the laser field strength stays low. Cionga et al. [24] use the Jacob-Anger of the exponential to gain a greater understanding of dressing effects.

$$\exp[ixsin(\omega t)] = \sum_{-\infty}^{+\infty} J_N(x)\exp(iN\omega t) \tag{6}$$

Here J_N is Bessel function, N is net number of photons that are exchanged (absorbed or released), ω is frequency, and t is time. This Equation (6) here acts as mathematical tools which is used to solve the complex integral part. The exchange of photon takes place when a projectile electron collides with a hydrogen atom in an environment of a monochromatic, single-mode, linear polarized laser field. For a process involving N photons, the DCS can be expressed as follows [25]:

$$\frac{d\sigma_N}{d\Omega} = (2\pi)^4\frac{k_f}{k_i}|T_N|^2 \tag{7}$$

T_N is general structure of the S-matrix element equation followed by the transition matrix element.

$$T_N = T_N^{(0)} + T_N^{(1)} + \ldots \tag{8}$$

And the first term is given by Dhankhar and Choubisa [26],

$$T_N^{(0)} = J_N(\vec{\alpha}\cdot\vec{q}) < \psi_{nlm}|F(\vec{q})|\psi_{nlm} > \tag{9}$$

The above equation corresponds to the Bunkin-Fedorov formula [6], where the laser dressing of the target is disregarded. Here, T_N simplifies to $T_N^{(0)}$, and ordinary Bessel functions $J_N(\vec{\alpha}\cdot\vec{q})$ encompass all the field dependencies of the transition matrix. An additional term arises from the atomic state dressing under a linearly polarized laser field. The form factor operator $F(\vec{q})$ can be expressed as $\vec{q} = \vec{k}_i - \vec{k}_f$.

$$F(\vec{q}) = \frac{1}{2\pi^2 q^2}[\exp(i\vec{q}\cdot\vec{r}) - 1] \tag{10}$$

For a linearly polarized electromagnetic field along the any one axis, the interaction potential can be written as:

$$V(t) = -er\cdot E(t) \tag{11}$$

$$E(t) = E_0\cos(\omega t - \phi)\,\hat{e}_p \tag{12}$$

where E is field strength of laser field, ϕ is phase angle [27]. Now to calculate the DCS for 1s-1s state, the transition matrix is obtained using relation $<\psi_{1,0,0}|F(\vec{q})|\psi^*_{1,0,0}>$ [28] in presence of laser field where wave function $\psi_{1,0,0}$ is being operated with form factor operator $F(\vec{q})$. The DCS cross-section from this transition and Equation (4) we get,

$$\frac{d\sigma_n}{d\Omega} = \frac{k_f}{k_i}\frac{1}{\pi^2 a_0^4 q^4} e^{\frac{-4r}{a_0}} \left| \left(\frac{iqa_0 cos\theta}{2\omega}\right)^n e^{in\theta} + 1 \right|^2 \tag{13}$$

where n is Bessel function order and energy shift for same state is obtained as:

$$\Delta E = e\left(\frac{1}{\pi}\right) E(t) \left(\frac{1}{a_0}\right)^3 \frac{1}{4} a_0 e^{-\frac{2r}{a_0}} (a_0 + 2r) \tag{14}$$

Similarly, for 2s state the DCS is obtained as:

$$\frac{d\sigma_n}{d\Omega} = \frac{k_f}{k_i}\frac{1}{2\pi^2 a_0^3 q^4} e^{\frac{-2r}{a_0}} \left(2a_0 - 2r + \frac{r^2}{a_0}\right)^2 \left| \left(\frac{iqa_0 cos\theta}{2\omega}\right)^n e^{in\theta} + 1 \right|^2 \tag{15}$$

For 2s, the energy shift is obtained as:

$$\Delta E = -\frac{1}{16\pi} E(t) e \left(-2a_0^2 - 2a_0 r + r^2 - \frac{r^3}{a_0}\right) e^{-\frac{r}{a_0}} \tag{16}$$

Also, for 3s state DCS is obtained as:

$$\frac{d\sigma_n}{d\Omega} = \frac{4k_f}{6561 k_i \pi^2 q^4 a_0^6} e^{-4r/3a_0} \left(729 - \frac{972r}{a_0} + \frac{432r^2}{a_0^2} - \frac{72r^3}{a_0^3} + \frac{4r^4}{a_0^4}\right)^2 \left| \left(\frac{iqa_0 cos\theta}{2\omega}\right)^n e^{in\theta} + 1 \right|^2 \tag{17}$$

For 3s state energy shift is obtained as:

$$\Delta E = -\left(\frac{1}{a_0}\right)^6 \left(\frac{eE(t)e^{-2r/3a_0}}{19683\pi}\right) \left(-\frac{64675a_0^5}{100} - \frac{3645a_0^4 r}{10} + 243a_0^3 r^2 - 1566a_0^2 r^2 + 63a_0 r^4 - 6r^5\right) \tag{18}$$

For $n = 2$ and $n = 3$, transition matrix is obtained using $<\psi_{3,0,0}|F(\vec{q})|\psi^*_{2,0,0}>$; this represents the DCS for 3s to 2s or 2s to 3s as above is obtained as:

$$\frac{d\sigma_n}{d\Omega} = \frac{k_f}{109350 k_i \pi^2 a_0^6 q^4} e^{\frac{-5r}{3a_0}} \left[\frac{9519a_0}{250} + \frac{87r}{5} + \frac{432a_0 r}{25} - \frac{22r^2}{a_0} + \frac{2r^3}{a_0^2}\right]^2 \left| \left(\frac{iqa_0 cos\theta}{2\omega}\right)^n e^{in\theta} + 1 \right|^2 \tag{19}$$

Also, the energy shifts with laser field with transition from 3s to the 2s state is obtained as:

$$\Delta E = \frac{1}{324\sqrt{5\pi}} \left(\frac{1}{a_0}\right)^3 e \cdot E(t) \left(\frac{44712a_0^2}{3125} + \frac{7452a_0 r}{625} - \frac{2754r^2}{125} + \frac{372r^3}{25a_0} - \frac{12r^4}{5a_0^2}\right) \tag{20}$$

Similarly, the DCS for 3s to 1s obtained as:

$$\frac{d\sigma_n}{d\Omega} = \frac{k_f}{k_i}\frac{1}{8748\pi^2 a_0^6 q^4} e^{\frac{-8r}{3a_0}} \left(\frac{63}{4}a_0 - 15r + \frac{2r^2}{a_0}\right)^2 \left| \left(i^n \frac{qa_0 cos\theta}{2\omega} e^{in\theta} + 1\right) \right|^2 \tag{21}$$

Also, the energy shifts due to laser field of 3s to 1s state transaction is obtained as:

$$\Delta E = \frac{1}{324\sqrt{5\pi}} \left(\frac{1}{a_0}\right)^3 e \cdot E(t) \left(\frac{44712a_0^2}{3125} + \frac{7452a_0 r}{625} - \frac{2754r^2}{125} + \frac{372r^3}{25a_0} - \frac{12r^4}{5a_0^2}\right) \tag{22}$$

Similarly, the DCS for 2s to 1s transition is obtained as:

$$\frac{d\sigma_N}{\Omega} = \frac{2}{9}\frac{k_f}{k_i}\frac{1}{\pi^2 a_0^6 q^4} e^{\frac{-3r}{a_0}} \left(\frac{4a_0}{3} - r\right)^2 \left| \left(i\frac{qa_0 cos\theta}{2\omega} e^{i\theta} + 1\right) \right|^2 \tag{23}$$

Also, the energy shifts for transition 2s to 1s state are obtained as:

$$\Delta E = -e\frac{1}{4\pi\sqrt{2}} \left(\frac{1}{a_0}\right)^3 E(t) \left(\frac{4}{9}a_0 r + \frac{16}{27}a_0^2 + \frac{18}{27}r^2\right) \tag{24}$$

3. Results and Discussion

3.1. Computational detail

The computational analysis was conducted using the student package of MATLAB, focusing on the interaction of laser photons with energy of 1.17 eV and electrons with energies up to 3 MeV. The electric field strength varied from 1 a.u. to 4 a.u., while the Bessel function order ranged from 1 to 4. The scattering angle was considered between 0 and 30 degrees, and the distance separation was set from 1 to 4 Å.

3.2. Differential cross section

The DCS for undressed scattering, focusing on elastic scattering transitions across various atomic states and incident energies, is shown in Figure 1. The DCS plots for transitions including the 1s-1s, 2s-2s, and 3s-3s states exhibit consistent trends characterized by exponential-like decay. In the 1s-1s state, we observed a rapid decrease in DCS as energy increased up to approximately 0.8 MeV, followed by a more gradual decline, stabilizing after 1.5 MeV. This stabilization suggests that the coulombic repulsion of the target in its ground state becomes increasingly weak at higher energies. Numerically, the initial rapid drop in DCS for the 1s-1s state up to 0.8 MeV reflects the strong initial interaction between the incident particle and the target due to coulombic repulsion. As energy increases beyond this threshold, the electron configuration stabilizes, leading to a more gradual decrease in DCS. This behavior indicates a transition towards a state where the interaction dynamics are less affected by initial repulsive forces and more by the electron's spatial distribution within the atom. In contrast, transitions involving higher orbital states such as 2s-2s and 3s-3s exhibit smoother,

Figure 1
DCS with change in momentum for different transition state

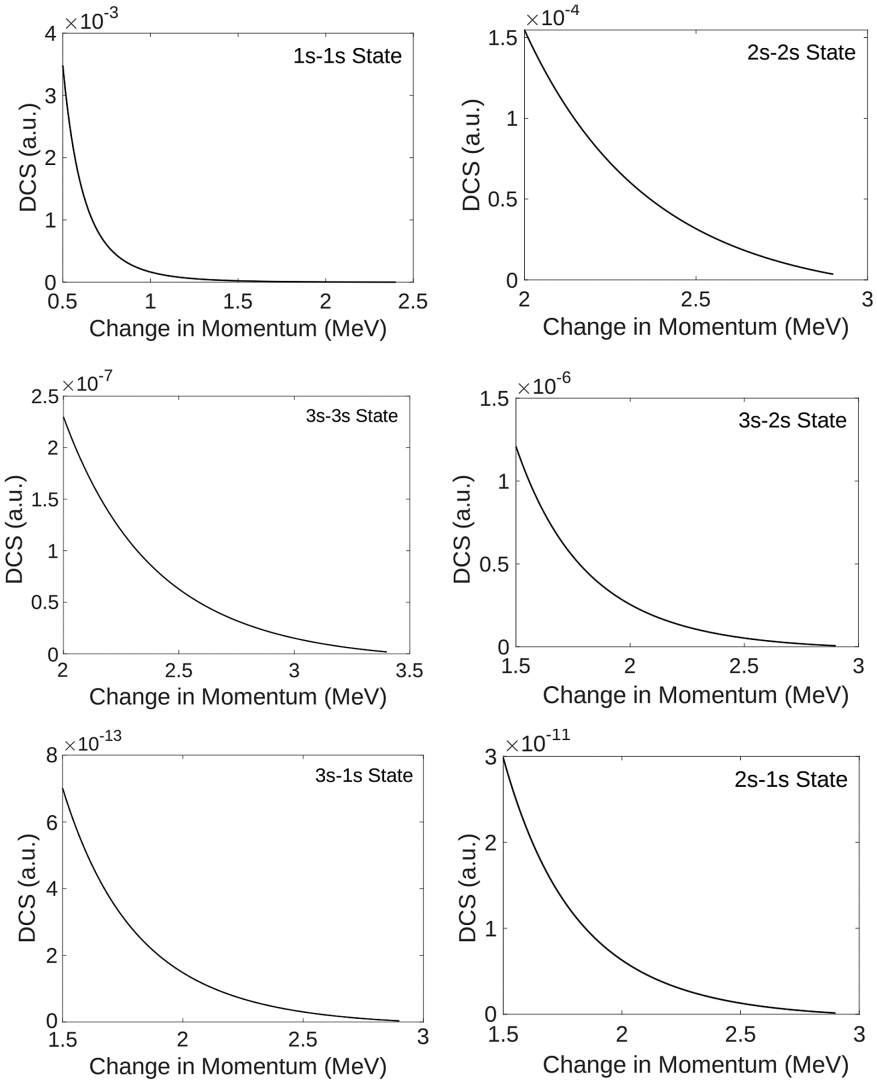

curved decreases in DCS across a wider range of momentum changes than the 1s-1s state. This broader range suggests that electrons in higher orbitals have larger spatial extents, influencing interaction dynamics over a more varied momentum spectrum. The observed behaviors in these transitions highlight the complexity introduced by electron distribution and interaction energies in determining the scattering characteristics.

Notably, transitions involving the 3s state, such as 3s-2s, demonstrate a pronounced decrease in DCS with increasing energy from 1.5 MeV to 2 MeV. Beyond 2.5 MeV, changes in momentum have minimal effects on DCS, indicating a near-equilibrium state where the coulombic repulsion of the target is increasingly balanced by the electron's projected influence. Similar trends are observed in transitions like 3s-1s and 2s-1s states, where momentum changes above 2.5 MeV show minimal impact on DCS, suggesting approaching equilibrium conditions in atomic interactions. Also, with increasing the energy beyond 3 MeV in general the DCS is found constant. These findings provide valuable insights into the fundamental atomic collision processes, highlighting the interplay between atomic structure, incident energy, and DCS behaviors. Understanding these interactions is crucial for applications in plasma physics, materials science, and other fields where precise modeling of atomic interactions under varying conditions is essential. Future research could explore additional atomic states and higher energy regimes to further elucidate the complex dynamics observed in DCS and their implications for broader scientific inquiries. Jablonski et al. [29] compared electron elastic scattering cross-sections estimated using two commonly used atomic potential and discovered that DSC decreases as energy increases for H, At, Ni, Ag, An, and Cm atoms. Our study has the same nature [29]. Silva et al. [30] also investigated the elastic along with electronically inelastic scattering of electrons through 2H-pyran and 4H-pyran molecules, discovering that the cross-section decreases as energy increases.

3.3. DCS with scattering angle

The findings indicate that the DCS decreases as the scattering angle decreases, which corresponds to an increase in the amplitude of the transition. This behavior is attributed to the properties of the Bessel function, as illustrated in Figure 2. When using a Bessel function of order 1, the oscillations are lower, but the amplitude

Figure 2
DCS with scattering angle

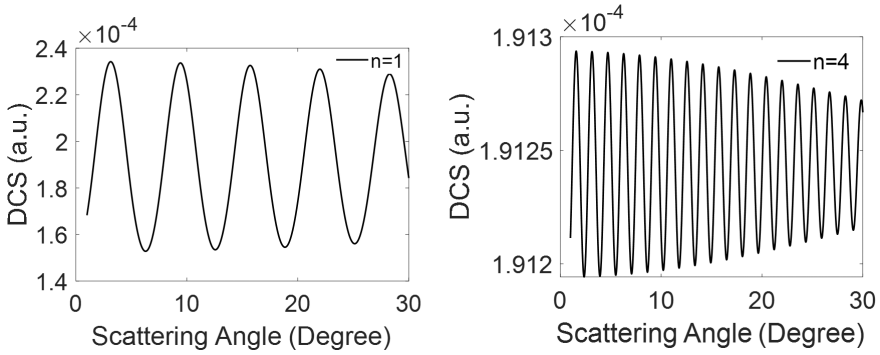

Figure 3
Energy shift with distance separated between target and project electron at different transition state

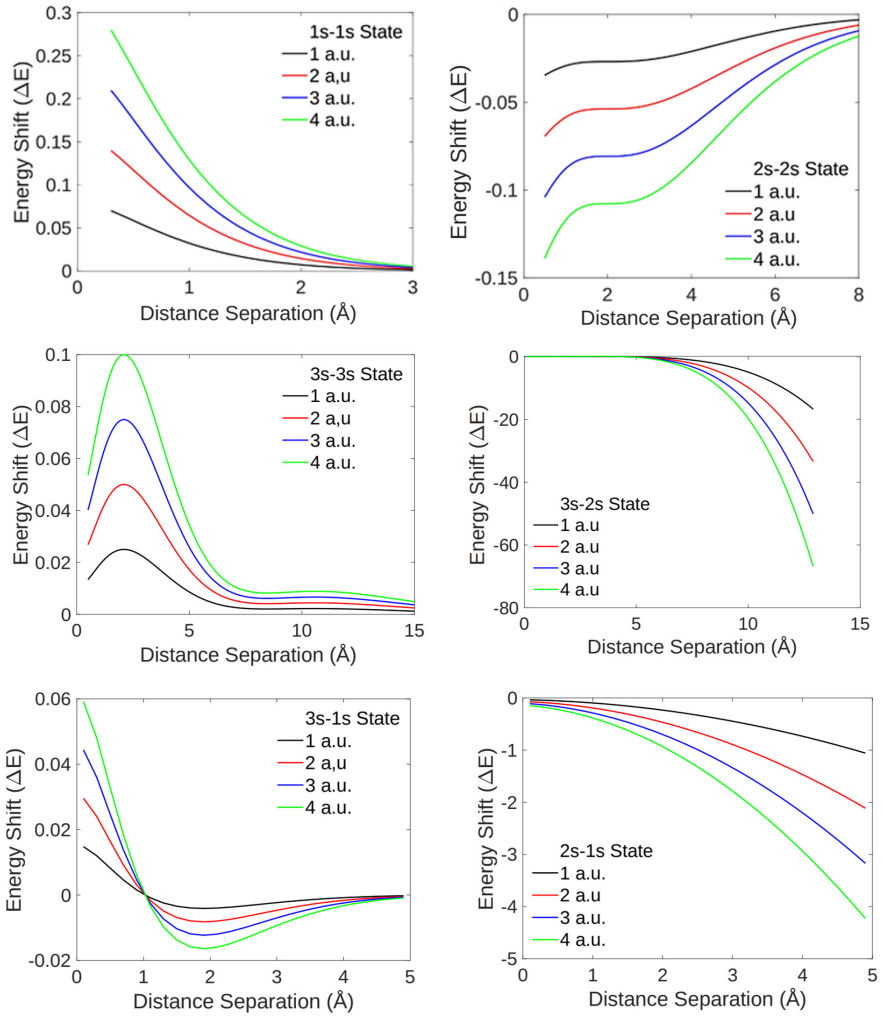

is higher. Conversely, with a Bessel function of order 4, the oscillations increase while the amplitude decreases with increasing scattering angles. This damping nature of the amplitude is a characteristic of the Bessel function and spreading of scattering probability over more directions, faster decay of higher-order terms, and possible destructive interference effects. The analysis reveals a distinct variation in DCS values based on the order of the Bessel functions used. Lower orders of Bessel functions tend to produce higher DCS values, which implies a significant impact on the angular scattering patterns governed by

these functions. As the order of the Bessel function increases, the angular dependence of scattering becomes more complex. This complexity reflects the intricate interference patterns and intensity distributions typical of elastic scattering phenomena.

These observations emphasize the crucial role of Bessel functions in shaping scattering behavior. The use of Bessel functions effectively describes and predicts the angular distributions in atomic and particle interactions. This highlights their utility in understanding and modeling the nuances of scattering processes, where lower-order Bessel functions are associated with higher amplitudes and simpler oscillation patterns, while higher-order functions exhibit increased oscillatory behavior but reduced amplitudes.

3.4. Energy shift with the application of laser field

The graphs presented depict the relationship between momentum change and distance separation, differentiated by the intensity of the time-dependent electric field. In these graphs, represented by black (1 a.u.), red (2 a.u.), blue (3 a.u.), and green (4 a.u.), higher values of electric field correspond to lower energy shift values, indicating a pronounced influence of the electric field intensity on the scattering dynamics across different atomic states as shown in Figure 3. In the 1s-1s state, the energy shift exhibits a sharp decrease with minimal increases in distance separation when subjected to higher electric field values (4 a.u.), compared to slower decreases observed at lower electric field values (1 a.u.). This behavior suggests that stronger electric fields induce more rapid changes in energy shift, reflecting the enhanced interaction between the projectile electron and the target atom. As distance increases, the energy shift initially shifts from negative to positive values, converging towards equilibrium around 8 eV, indicative of the stabilization of interaction forces.

In the 2s-2s state, higher values of electric field lead to lower energy shift values, indicating a more significant influence of the electric field intensity on reducing energy shifts across various distances. Similar to the 1s-1s state, as distance increases, the energy shift transitions gradually from negative to positive values, showing a steady decrease in energy shift with increasing distance. In contrast, the 3s state exhibits a notable increase in energy shift at smaller distances, particularly evident with higher values of electric field. This suggests that the electric field intensity amplifies the initial energy shift at closer distances, while diminishing effects are observed as distance increases towards 8 angstroms, where convergence towards similar energy shift values occurs.

The transition states like 3s-2s and 3s-1s highlight distinct behaviors influenced by electric field. For instance, in the 3s-2s state, higher electric field values result in rapid initial decreases in energy shift compared to slower decreases at lower electric field values. Conversely, in the 3s-1s state, higher electric field values lead to more pronounced reductions in energy shift, with converging behaviors observed around 1 angstrom. This is because at this distance the destructive interference take place and result shifting is zero due to a larger transition gap between 3s-1s.

4. Conclusion

The computational analysis of the developed theoretical model has demonstrated that the DCS and energy shifts are significantly influenced by various parameters, such as electron distribution, energy, electric field strength, and Bessel function orders. DCS is primarily affected by electron orbital states and scattering angles, with lower-order Bessel functions producing simpler patterns and higher orders introducing more complex oscillations. The DCS decreases more rapidly in the ground state and stabilizes over time, while higher orbital states exhibit smoother transitions due to their larger electron distributions. Conversely, energy shifts are mainly influenced by electric field intensity, with stronger fields causing rapid shifts at shorter distances and stabilizing over larger separations. These interactions underscore the critical role of these parameters in understanding atomic collision dynamics.

Ethical Statement

This study does not contain any studies with human or animal subjects performed by any of the authors.

Conflicts of Interest

The authors declare that they have no conflicts of interest to this work.

Data Availability Statement

Data are available from the corresponding author upon reasonable request.

Author Contribution Statement

Raju Bohora: Conceptualization, Methodology, Software, Formal analysis, Investigation, Resources, Data curation, Writing – original draft, Visualization. **Kishori Yadav:** Validation, Writing – review & editing, Supervision, Project administration. **Saddam Husain Dhobi:** Conceptualization, Methodology, Software, Formal analysis, Investigation, Resources, Data curation, Writing – original draft, Visualization.

References

[1] Bartschat, K., Tennyson, J., & Burke, P. (2023). Electron–atom, electron–ion, and electron–molecule collisions. In G. W. F. Drake (Ed.), *Springer handbook of atomic, molecular, and optical physics* (pp. 725–750). Springer. https://doi.org/10.1007/978-3-030-73893-8_49

[2] Lévêque-Simon, K., & Hervieux, P. A. (2023). Antihydrogen formation from laser-assisted antiproton-positronium collisions. *Physical Review A*, *107*(5), 052813. https://doi.org/10.1103/PhysRevA.107.052813

[3] Chen, Z. B. (2023). Electron-impact excitation of atoms or ions with the screened Coulomb potential. *Physics of Plasmas*, *30*(3), 032103. https://doi.org/10.1063/5.0140534

[4] Ishikawa, M., Ishida, K., Kanya, R., & Yamanouchi, K. (2023). Angle-resolved time-of-flight electron spectrometer designed for femtosecond laser-assisted electron scattering and diffraction. *Instruments*, *7*(1), 4. https://doi.org/10.3390/instruments7010004

[5] Synanidis, A. P., Gonçalves, P. A. D., Ropers, C., & de Abajo, F. J. G. (2024). Quantum effects in the interaction of low-energy electrons with light. *Science Advances*, *10*(25), eadp4096. https://doi.org/10.1126/sciadv.adp4096

[6] Bunkin, F. B., Kazakov, A. E., & Fedorov, M. V. (1973). Interaction of intense optical radiation with free electrons (nonrelativistic case). *Soviet Physics Uspekhi*, *15*(4), 416. https://doi.org/10.1070/PU1973v015n04ABEH004990

[7] Kroll, N. M., & Watson, K. M. (1973). Charged-particle scattering in the presence of a strong electromagnetic wave. *Physical Review A*, *8*(2), 804–809. https://doi.org/10.1103/PhysRevA.8.804

[8] Mason, N. J. (1993). Laser-assisted electron-atom collisions. *Reports on Progress in Physics*, *56*(10), 1275. https://doi.org/10.1088/0034-4885/56/10/002

[9] Gersten, J. I., & Mittleman, M. H. (1976). Electron scattering from atoms in the presence of a laser field. *Physical Review A*, *13*(1), 123–130. https://doi.org/10.1103/PhysRevA.13.123

[10] Zon, B. A. (1977). Bremsstrahlung in collisions between electrons and atoms. *Journal of Experimental and Theoretical Physics*, *46*(1), 65–68.

[11] Beilin, E. L., & Zon, B. A. (1983). On the sum rule for multiphoton bremsstrahlung. *Journal of Physics B: Atomic and Molecular Physics*, *16*(6), L159. https://doi.org/10.1088/0022-3700/16/6/003

[12] Francken, P., & Joachain, C. J. (1990). Theoretical study of electron–atom collisions in intense laser fields. *Journal of the Optical Society of America B*, *7*(4), 554–563. https://doi.org/10.1364/JOSAB.7.000554

[13] Chin, S. L. (2012). *Multiphoton ionization of atoms*. USA: Academic Press.

[14] Dhobi, S. H., Yadav, K., Jha, A. K., Karki, B., & Nakarmi, J. J. (2022). Free electron-ion interaction and its effect on output current of permeable exchange membrane hydrogen fuel. *ECS Transactions*, *107*(1), 8457–8468. https://doi.org/10.1149/10701.8457ecst

[15] Dhobi, S. H., Pudasaini, A., Oli, D., Khatiwada, S., Ghimire, K., Rijal, O. S., . . . , & Paudel, G. (2024). Scattering of free electrons with hydrogen atoms in proton exchange membrane fuel cell. *Hadronic Journal*, *47*(1), 1–14.

[16] Jacob, A. (2024). Radiation-field-driven ionization in laser-assisted slow atomic collisions. In A. Jacob (Ed.), *Relativistic effects in interatomic ionization processes and formation of antimatter ions in interatomic attachment reactions* (pp. 51–85). Springer. https://doi.org/10.1007/978-3-658-43891-3_3

[17] Kanti, D., Majczak, M. M., Kamiński, J. Z., Peng, L. Y., & Krajewska, K. (2024). Laser-assisted radiative recombination beyond the dipole approximation. *Physical Review A*, *110*(4), 043112. https://doi.org/10.1103/PhysRevA.110.043112

[18] Ehlotzky, F., Krajewska, K., & Kamiński, J. Z. (2009). Fundamental processes of quantum electrodynamics in laser fields of relativistic power. *Reports on Progress in Physics*, *72*(4), 046401. https://doi.org/10.1088/0034-4885/72/4/046401

[19] Mandal, A., Dhankhar, N., Sébilleau, D., & Choubisa, R. (2021). Semirelativistic (e, 2e) study with a twisted electron beam on Cu and Ag. *Physical Review A*, *104*(5), 052818. https://doi.org/10.1103/PhysRevA.104.052818

[20] Cionga, A., Ehlotzky, F., & Zloh, G. (2001). Elastic electron scattering by excited hydrogen atoms in a laser field. *Physical Review A*, *64*(4), 043401. https://doi.org/10.1103/PhysRevA.64.043401

[21] Dhankhar, N., Banerjee, S., & Choubisa, R. (2022). Twisted electron impact single ionization coincidence cross-sections for noble gas atoms. *Journal of Physics B: Atomic, Molecular and Optical Physics*, *55*(16), 165202. https://doi.org/10.1088/1361-6455/ac7d80

[22] Jiang, S., Gudem, M., Kowalewski, M., & Dorfman, K. (2024). Multidimensional high-harmonic echo spectroscopy: Resolving coherent electron dynamics in the EUV regime. *Proceedings of the National Academy of Sciences*, *121*(7), e2304821121. https://doi.org/10.1073/pnas.2304821121

[23] Kovačević, S., Čerkić, A., Busuladžić, M., & Milošević, D. B. (2020). Electron-atom potential scattering in a corotating bicircular laser field. *Laser Physics*, *30*(5), 055301. https://doi.org/10.1088/1555-6611/ab8473

[24] Cionga, A., Ehlotzky, F., & Zloh, G. (2000). Electron-atom scattering in a circularly polarized laser field. *Physical Review A*, *61*(6), 063417. https://doi.org/10.1103/PhysRevA.61.063417

[25] Mondal, M., Mandal, B., Haque, A., Purkait, K., & Purkait, M. (2024). Theoretical triple differential cross sections for ionization of N_2 and CH_4 molecules by electron impact. *Physica Scripta*, *99*(5), 055409. https://doi.org/10.1088/1402-4896/ad3e42

[26] Dhankhar, N., & Choubisa, R. (2022). Triple-differential cross section for the twisted-electron-impact ionization of the water molecule. *Physical Review A*, *105*(6), 062801. https://doi.org/10.1103/PhysRevA.105.062801

[27] Madsen, L. B. (2022). Nondipole effects in tunneling ionization by intense laser pulses. *Physical Review A*, *105*(4), 043107. https://doi.org/10.1103/PhysRevA.105.043107

[28] Singh, K., & Singh, S. P. (2005). *Elements of quantum mechanics*. India: S. Chand Publishing.

[29] Jablonski, A., Salvat, F., & Powell, C. J. (2004). Comparison of electron elastic-scattering cross sections calculated from two commonly used atomic potentials. *Journal of Physical and Chemical Reference Data*, *33*(2), 409–451. https://doi.org/10.1063/1.1595653

[30] Silva, M. O., Moreira, G. M., Bettega, M. H. F., & da Costa, R. F. (2024). Elastic and electronically inelastic scattering of electrons by 2H-pyran and 4H-pyran molecules. *Journal of Applied Physics*, *135*(2), 024702. https://doi.org/10.1063/5.0187724

How to Cite: Bohora, R., Yadav, K., & Dhobi, S. H. (2025). Differential Cross-Sections and Energy Shifts in Electron-Atom Scattering Under Linearly Polarized Laser Fields. *Journal of Optics and Photonics Research*, *2*(2), 86–92. https://doi.org/10.47852/bonviewJOPR42023979